

**Infrared emission spectra of fullerene C<sub>60</sub> thin films**Tomonari Wakabayashi \* and Hal Suzuki*Department of Chemistry, Kindai University, Higashi-Osaka 577-8502, Japan*

Miho Hatanaka

*Department of Chemistry, Keio University, Yokohama 223-8522, Japan*

Hiroyuki Wakabayashi

*Department of Physics, Osaka University, Toyonaka 560-0043, Japan*Takeshi Kodama *Kanagawa Institute of Technology, Atsugi 243-0292, Japan*

(Received 3 September 2023; revised 29 October 2023; accepted 8 December 2023; published 10 January 2024)

Infrared (IR) spectra of thin films of fullerene C<sub>60</sub> molecules of icosahedral ( $I_h$ ) symmetry are recorded as thermal emission of radiation at elevated temperatures in the range of 27 °C–88 °C. Temperature dependence is analyzed for relative intensities of four IR-active emission bands of vibrational  $T_{1u}$  modes of C<sub>60</sub>. Theoretical simulations are performed on the basis of the temperature-dependent thermal population of vibrationally excited states in a C<sub>60</sub> molecule, counting explicitly the number of overtones and combinations for all possible energy levels by the excitation of up to seven vibrational quanta. The observed IR emission intensity increases with increasing temperature for all the bands of  $T_{1u}(i)$ , with  $i = 1-4$ , at 526, 575, 1182, and 1427 cm<sup>-1</sup>, whereas the intensity of higher-frequency modes,  $T_{1u}(3)$  and  $T_{1u}(4)$ , increases more drastically than that of  $T_{1u}(1)$  and  $T_{1u}(2)$ . The analyses show clearly how and why the IR emission spectrum of C<sub>60</sub> changes with temperature. For the thick sample of C<sub>60</sub>, saturation of the IR emission bands is observed due to self-absorption. The molecular IR emission of C<sub>60</sub> is shown to be an ideal system for consideration of the vibrational temperature and an appropriate probe for astrophysical conditions of cosmic C<sub>60</sub> molecules.

DOI: [10.1103/PhysRevB.109.035409](https://doi.org/10.1103/PhysRevB.109.035409)**I. INTRODUCTION**

The series of events concerning discoveries related to fullerene C<sub>60</sub> has led to important milestones in molecular physics, materials science, and astrophysics [1–7]. In 1985, laser-vaporized graphite in a supersonic jet of helium gas as an experimental study motivated by the desire to reproduce interstellar conditions led to the discovery of superstable clusters of C<sub>60</sub> and C<sub>70</sub> by mass spectrometry, and the hollow closed-cage molecule of carbon was coined buckminsterfullerene [1]. In 1990, resistive heating of graphite to prepare carbon soot aimed at mimicking cosmic dust was found to be a method capable of producing macroscopic amounts of C<sub>60</sub> [2]. Infrared (IR) spectroscopy played a crucial role in the confirmation of the presence of the highly symmetric molecule of C<sub>60</sub> [3]. The infrared space telescope Spitzer/IRS opened the way beyond microwave spectroscopy in radio astronomy to confirm the existence of nonpolar molecules of C<sub>60</sub> and C<sub>70</sub> in a young planetary nebula in 2010 [4]. Eventually, ionized fullerene C<sub>60</sub><sup>+</sup> was confirmed as a carrier of some diffuse interstellar bands by helium-tagging spectroscopy in 2015 [5], long after the proposal in 1994 [6]. It has been a half-century journey

since the prediction of aromatic stability of a carbon molecule with the shape of a truncated icosahedron in 1970 [7].

With solid-state samples of C<sub>60</sub>, four bands in the IR absorption spectra have been studied extensively under various conditions and compared with theoretical vibrational mode frequencies of the molecule [8–10]. As far as we know, the first report of IR emission spectra using thin films of solid C<sub>60</sub> focused on chemical analyses of thermal stability and oxidation of the molecule at 100 °C–600 °C [11]. The IR emission spectra of gas phase C<sub>60</sub> molecules were recorded at high temperatures above 600 °C, revealing broadband spectra with the rotation-vibration contour for the four IR-active  $T_{1u}$  modes [12,13]. Following the detection of the IR emission bands of fullerene C<sub>60</sub> in a young planetary nebula in 2010 [4], they have been confirmed in many objects in the late stages of stellar evolution such as postasymptotic giant branch stars, protoplanetary nebulae, planetary nebulae, reflection nebulae, and young stellar objects [14–21] by observations using the same satellite observatory, and a discussion of the formation mechanism of fullerenes in space has taken place [22–24].

One of the key questions surrounding cosmic fullerene C<sub>60</sub> is the excitation mechanism, for which thermal emission [4] and UV-induced fluorescent IR emission [15] are under debate [25]. Prior to emitting an IR photon, the C<sub>60</sub> molecule must be

\*wakaba@chem.kindai.ac.jp

lifted to the vibrationally excited state. The thermal emission model requires equilibrium vibrational temperatures around 330 K to reproduce the observed ratios for the IR-active vibrational emission band intensities [4]. It is natural to consider that the relative IR emission band intensity between the modes of different vibrational frequencies changes via vibrational temperature and is used as a probe of the physical and chemical conditions as well as the abundance of the molecule in space [26,27]. The IR *absorption* spectra of C<sub>60</sub> and related compounds have been examined even at high temperatures [28,29]. Concerning the IR *emission* spectra of C<sub>60</sub>, experimental works have been less explored following the three initial reports [11–13]. For the IR emission spectroscopy at elevated temperatures, statistical treatments including transitions between two vibrationally excited states, namely, *hot bands*, are necessary.

The purpose of this work is to provide a systematic view to understand how and why the IR emission spectrum of C<sub>60</sub> changes with temperature. First, IR emission spectra of a thin film of fullerene C<sub>60</sub> are measured in a temperature range of 300–360 K, and systematic changes in the relative intensities of the four IR-active vibrational modes are analyzed. We take advantage of the solid-state sample of C<sub>60</sub> thin films containing a sufficient number of molecules in a small volume under the spectroscopic probe. With the closely packed structure of C<sub>60</sub> molecules in a condensed phase, the amount of material is kept constant during the series of measurements at different temperatures; therefore, quantitative analyses of the spectral intensity become feasible. Relatively weak interaction between molecules in the molecular crystal of C<sub>60</sub> justifies interpretation of spectra with molecular properties for individual molecules. Second, theoretical simulations are conducted for the spontaneous emission intensities of the four IR-active vibrational modes of C<sub>60</sub> in a temperature range of 50–400 K by explicitly taking all possible vibrationally excited states, namely, fundamentals, overtones, and combinations, into consideration with excitations by one to seven vibrational energy quanta.

## II. EXPERIMENTS

Before emission spectra were measured, an absorption spectrum was measured by using a Fourier transform IR spectrometer for a thin film of C<sub>60</sub> molecules deposited on a transparent disk of potassium bromide to estimate the amount of material from the thickness of the film. The IR emission spectra of the C<sub>60</sub> sample were recorded on the same spectrometer. The Supplemental Material includes experimental details in Figs. S1 and S2, together with theoretical and experimental information in Tables SI–SIII [30].

For the intensity calibration, the C<sub>60</sub> sample was replaced by a graphite disk, and its thermal emission spectra were recorded at the relevant range of temperatures. The spectrum of graphite was used for conversion from spectral intensity to energy density as blackbody radiation. After the background correction, the spectra  $I_{C_{60}}(\tilde{\nu}, T)$  for C<sub>60</sub> and  $I_G(\tilde{\nu}, T)$  for graphite were adopted as follows:

$$\sigma(\tilde{\nu}, T)d\tilde{\nu} = \frac{I_{C_{60}}(\tilde{\nu}, T)}{I_G(\tilde{\nu}, T)} \frac{8\pi hc\tilde{\nu}^3}{e^{\frac{hc\tilde{\nu}}{kT}} - 1} d\tilde{\nu}, \quad (1)$$

where the spectrum  $\sigma(\tilde{\nu}, T)$  has the dimension of energy flux (in J m<sup>-2</sup>). For the use of the wave number  $\tilde{\nu}$  (in cm<sup>-1</sup>) as the variable,  $\sigma(\tilde{\nu}, T)$  is presented here as energy density per wave number (J m<sup>-3</sup> cm); therefore, integrated intensity over the wave number  $\tilde{\nu}$  (in cm<sup>-1</sup>) is given by energy density (in J m<sup>-3</sup>). This definition of energy-based spectral intensity contrasts with the dimensionless normalization, which provides emission spectra closely resembling absorption spectra [11].

## III. THEORY

### A. Spontaneous emission rate and band strength

The theoretical framework is given here based on SI units, and the wave number  $\tilde{\nu}$ , which is proportional to the frequency of radiation,  $\nu = c\tilde{\nu}$ , is chosen as the variable. The contribution of induced emission by ambient infrared radiation is neglected for simplicity, and only spontaneous emission is taken into consideration. The degeneracy of the vibrational level is counted separately for each state in the level throughout the following formulation.

Einstein's  $A$  coefficient for spontaneous emission of radiation (in s<sup>-1</sup>) between two eigenstates from the upper  $j$  state to the lower  $k$  state is given by the formula

$$A_{jk} = \frac{16\pi^3 \tilde{\nu}^3}{3\epsilon_0 h} \sum_{\rho} |\langle j | \mu_{\rho} | k \rangle|^2, \quad (2)$$

whereas the  $B$  coefficient for induced emission (in m<sup>2</sup> J<sup>-1</sup> s<sup>-1</sup>) is as follows:

$$B_{jk} = \frac{2\pi^2}{3\epsilon_0 h^2 c} \sum_{\rho} |\langle j | \mu_{\rho} | k \rangle|^2, \quad (3)$$

where  $\mu_{\rho}$  denotes the electric dipole operator (in C m) and summation is taken over three directions of the electric dipole,  $\rho = x, y, z$  [31–35]. The symbols  $\epsilon_0$ ,  $h$ , and  $c$  denote the dielectric constant, Planck's constant, and speed of light, respectively. From the definition of Eqs. (2) and (3), the relation holds between  $A_{jk}$  and  $B_{jk}$  as

$$A_{jk} = 8\pi hc\tilde{\nu}^3 B_{jk}. \quad (4)$$

The band strength  $S_{kj}$  for the transition from the lower  $k$  state to the upper  $j$  state is defined by Napierian absorbance through the  $B$  coefficients for induced absorption and emission [34–36],  $B_{kj} = B_{jk}$ , as

$$S_{kj} = \frac{1}{Nl} \int_{\text{band}} \ln\left(\frac{I_0}{I}\right) d\tilde{\nu} = N_A h \tilde{\nu} B_{jk}, \quad (5)$$

where  $Nl$  denotes the column density of the molecule (in mol m<sup>-2</sup>). The spontaneous emission rate  $A_{jk}$  (in s<sup>-1</sup>) is then associated with the band strength for absorption,  $S_{kj} = I_{\text{IR}}$  (in m mol<sup>-1</sup>), as

$$A_{jk} = \frac{8\pi c \tilde{\nu}^2}{N_A} S_{kj} = 1.25 \times 10^{-14} \tilde{\nu}^2 I_{\text{IR}}, \quad (6)$$

provided that the vibrational frequency  $\tilde{\nu}$  is in units of m<sup>-1</sup>, where the constant is  $8\pi c/N_A = 1.25 \times 10^{-14}$  m s<sup>-1</sup> mol. For conventional units of cm<sup>-1</sup> for  $\tilde{\nu}$  and km mol<sup>-1</sup> for  $I_{\text{IR}}$ , the order factor  $10^{-14}$  is simply replaced by  $10^{-7}$ . This gives

TABLE I. The spontaneous IR emission rates  $A_{jk}$  for the four  $T_{1u}$  modes of  $C_{60}$ . Harmonic vibrational mode frequencies  $\tilde{\nu}$  and band strengths  $I_{IR}$  are obtained from molecular orbital calculations, using B3LYP/6-31G(d) in GAUSSIAN 16, revision C.01. Numbers in parentheses are the band strength multiplied by 3, the degeneracy of the  $T_{1u}$  mode.

Mode	$\tilde{\nu}$ (cm <sup>-1</sup> )	$I_{IR}$ (km mol <sup>-1</sup> )	$A_{jk}$ (s <sup>-1</sup> )
$T_{1u}(1)$	539	28.2 (84.6)	1.02
$T_{1u}(2)$	589	11.3 (33.9)	0.49
$T_{1u}(3)$	1215	9.0 (27.0)	1.66
$T_{1u}(4)$	1461	11.8 (35.4)	3.16

an estimation of the spontaneous emission rate for an excited state for one of the four  $T_{1u}$  modes of a  $C_{60}$  molecule using the frequency  $\tilde{\nu}$  and the band strength  $I_{IR}$ . Table I compares spontaneous emission rates of the four  $T_{1u}$  modes of  $C_{60}$  as estimated from theoretical mode frequencies and band strengths.

For comparison with the emission band intensity in an energy scale, the transition probability per molecule in the corresponding excited state in unit time, namely,  $A_{jk}$ , is converted to the emission energy per second per mole,  $\rho(\tilde{\nu})$  in J s<sup>-1</sup> mol<sup>-1</sup>, as

$$\rho(\tilde{\nu}) = N_A h c \tilde{\nu} A_{jk}. \quad (7)$$

This quantity,  $\rho(\tilde{\nu})$ , or at least its relative intensity can be compared with the experimental integrated emission band intensity [see Eq. (1)], which is calibrated for blackbody radiation (in J m<sup>-3</sup>),

$$\rho_{\text{exp}}(\tilde{\nu}, T) = \int_{\text{band}} \sigma(\tilde{\nu}, T) d\tilde{\nu}. \quad (8)$$

For temperature-dependent emission energy per second per mole, the theoretical quantity  $\rho(\tilde{\nu})$  is multiplied by a factor of probability for the population of molecules in IR-emissive vibrationally excited states for a particular IR-active  $T_{1u}$  mode.

### B. Vibrationally excited states of $C_{60}$

The  $C_{60}$  molecule with  $I_h$  symmetry has 46 distinct normal modes of vibration, including four IR-active modes with  $T_{1u}$  symmetry with threefold degeneracy, for which harmonic frequencies and band strengths are theoretically calculated:

$$\Gamma_{\text{vib}} = 2A_g + 3T_{1g} + 4T_{2g} + 6G_g + 8H_g + A_u + 4T_{1u} + 5T_{2u} + 6G_u + 7H_u. \quad (9)$$

Harmonic frequencies calculated for these modes are distributed in the range of 266–1618 cm<sup>-1</sup>, including those at 539, 589, 1215, and 1461 cm<sup>-1</sup> for the four IR-active  $T_{1u}$  modes. Table SI compiles the vibrational mode symmetry, degeneracy, harmonic frequency, and IR band strength for the 46 distinct normal modes of a  $C_{60}$  molecule obtained from the molecular orbital calculation at the B3LYP/6-31G(d) level of density functional theory using the Becke three parameter hybrid functional and the valence double zeta plus polarization basis set [37], which are used for simulations throughout the present work [30].

TABLE II. Degeneracy of vibrational levels for fundamentals and overtones in the icosahedral symmetry.

$v$	$A(1)$	$E(2)$	$T(3)$	$G(4)$	$H(5)$
0	1	1	1	1	1
1	1	2	3	4	5
2	1	3	6	10	15
3	1	4	10	20	35
4	1	5	15	35	70
5	1	6	21	56	126
6	1	7	28	84	210
7	1	8	36	120	330

The degeneracy of a vibrational level is associated with the number of patterns for distribution of vibrational quanta into degenerate states of the vibrational level. For example, for a  $T_{1u}$  mode with threefold degeneracy, the doubly excited level has sixfold degeneracy, as indicated by the direct product  $T_{1u} \times T_{1u} = A_g + H_g$ . Among three possible symmetry species in the direct product, the missing or vanishing one, namely,  $T_{1g}$  with threefold degeneracy, is called *antisymmetric* (see Appendix A). The six degrees of freedom corresponding to *symmetric* products, i.e., one nondegenerate  $A_g$  and one  $H_g$  with fivefold degeneracy, are associated with the number of distribution patterns of two vibrational quanta into three components of the degenerate  $T_{1u}$  vibrational mode, namely,  $(T_{1u}^{(x)}, T_{1u}^{(y)}, T_{1u}^{(z)}) = (2, 0, 0)$ ,  $(0, 2, 0)$ ,  $(0, 0, 2)$ ,  $(1, 1, 0)$ ,  $(1, 0, 1)$ , and  $(0, 1, 1)$ .

Table II lists the degeneracy of vibrational levels for fundamentals and overtones, where numbers in parentheses are degeneracies for the single-quantum fundamental excitation,  $v = 1$ . In general, degeneracies for overtones with excitation by  $v$  vibrational energy quanta are unity for all the levels for a nondegenerate  $A$  mode, whereas those for the others are calculated as  $v + 1$  for a doubly degenerate  $E$  mode,  $(v + 1)(v + 2)/2$  for a triply degenerate  $T$  mode,  $(v + 1)(v + 2)(v + 3)/6$  for a fourfold  $G$  mode, and  $(v + 1)(v + 2)(v + 3)(v + 4)/24$  for a fivefold  $H$  mode.

Symmetry species for overtones with excitation by  $v$  vibrational energy quanta of a  $T_{1u}$  mode of threefold degeneracy are reduced to a group of irreducible representations in  $(v + 1)(v + 2)/2$  total states [38,39]. Table III summarizes the vibrational species for overtones of a  $T_{1u}$  mode. For a vibrationally excited level with excitation of at least one

TABLE III. Symmetry species of vibrational levels for the fundamentals and overtones of the  $T_{1u}$  mode.

$v$	Degeneracy	Symmetry Species
0	1	$A_g$
1	3	$T_{1u}$
2	6	$A_g + H_g$
3	10	$T_{1u} + T_{2u} + G_u$
4	15	$A_g + G_g + 2H_g$
5	21	$2T_{1u} + 2T_{2u} + G_u + H_u$
6	28	$2A_g + T_{1g} + 2G_g + 3H_g$
7	36	$3T_{1u} + 3T_{2u} + 2G_u + 2H_u$

fundamental or overtone of a  $T_{1u}$  mode, every state within the degeneracy of the level has a chance to emit an IR photon equally via the electric dipole transition to one of the lower states since every upper state has a counterpart in the lower level which has an appropriate vibrational symmetry for the allowed transition.

In contrast to overtones, degeneracy for combinations of different vibrational modes is simply a product of degeneracies for corresponding modes. For fullerene  $C_{60}$  with  $I_h$  symmetry, the number of vibrational states increases with the increase of the number of energy quanta for vibrational excitation. The  $3N - 6 = 174$  vibrational degrees of freedom for a  $C_{60}$  molecule are classified into 46 distinct normal modes of the different vibrational frequencies and of the one-, three-, four-, or fivefold degeneracy as in Table SI [30].

The number of vibrationally excited levels with  $v = 1-7$  vibrational energy quanta composed of 46 distinct normal modes of a  $C_{60}$  molecule is listed in Table SII [30]. As a result, a total of 1 122 841 784 627 vibrationally excited states including degeneracy are found for 154 143 079 distinct vibrational energy levels of 46 fundamentals and their overtones and combinations. The numbers in parentheses in Table SII, e.g., (2,1,1), indicate the number of vibrational energy quanta for the excitation of a mode in the 46 normal modes; that is, “2” corresponds to a doubly excited mode, and “1” corresponds to a singly excited mode [30]. In the  $N$  column in Table SII, the number of patterns for the distribution of vibrational quanta into the 46 vibrational modes is listed, e.g.,  $46!/(46-3)!/3!/1!/2! = 45\,540$  patterns for the distribution of four quanta into three modes in the (2,1,1) manner [30].

By programming with C++, all these levels are listed together with vibrational frequencies and degeneracies, then converted to the vibrational density of states (DOS) as a function of the excitation energy up to  $12\,000\text{ cm}^{-1}$  with increments of  $1\text{ cm}^{-1}$ . Concerning the mode-selective DOS for IR-emissive states, namely, a state with excitation of at least one  $T_{1u}$  mode, the count of a state with multiple excitations of more than one  $T_{1u}$  mode is divided into fractions according to the weights of the rate of spontaneous emission of relevant  $T_{1u}$  modes (see Appendix B).

### C. IR-emissive state distribution at elevated temperature

The major concern about IR emission intensity at elevated temperature is the fraction of vibrationally excited states from which an IR photon can be emitted by an electric dipole transition or spontaneous emission. Under the principle of equal weights, Boltzmann distribution is applied to possible vibrational states, including the ground state, at a given temperature, and the partition function is calculated among all the states involved. From the probability distribution of vibrational states, populations of IR-emissive states are accumulated mode selectively and converted to the emission intensity proportional to a cube of the transition frequency and the band strength [see Eqs. (6) and (7)].

After summing emission intensities over all the IR-emissive vibrationally excited states for a particular mode, namely,  $T_{1u}(i)$ , with  $i = 1-4$ , the mode-selective emission band intensity is obtained. In other words, the

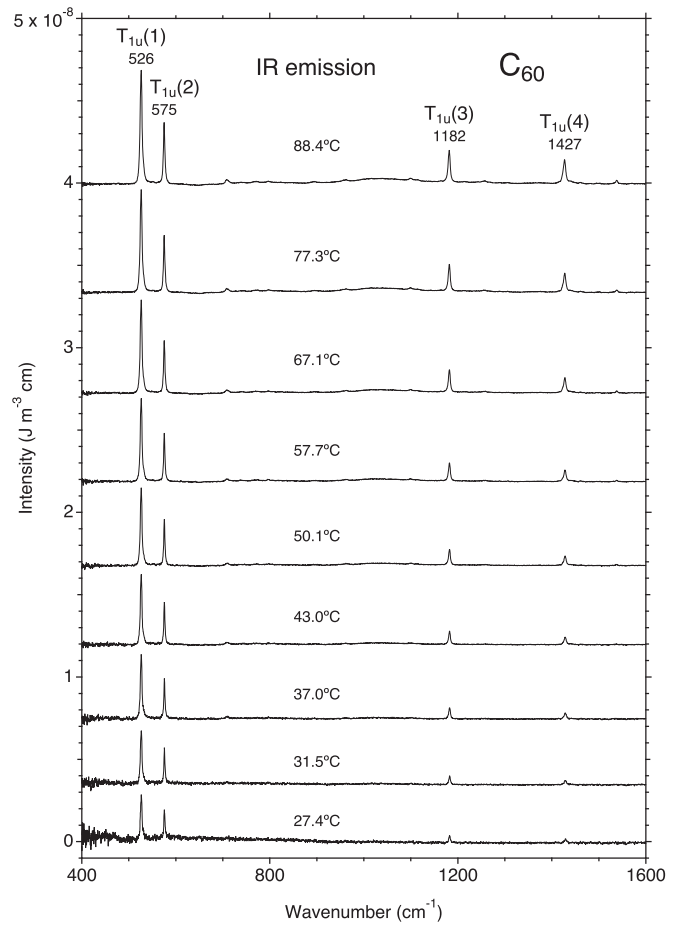


FIG. 1. IR emission spectra of the  $C_{60}$  thin film at various temperatures.

temperature-dependent mode-selective IR emission intensity  $\rho_i(\tilde{\nu}, T)$  is calculated in units of  $\text{J s}^{-1} \text{mol}^{-1}$  as a product of the spontaneous emission rate multiplied by the photon energy  $\rho_i(\tilde{\nu})$  and the excited-state population function  $f_i(T)$ , namely,  $\rho_i(\tilde{\nu}, T) = \rho_i(\tilde{\nu})f_i(T)$ .

## IV. RESULTS

### A. Experimental results

The thickness of the  $C_{60}$  film used in the present work is estimated to be  $d = 0.54\ \mu\text{m}$ , equivalent to  $\sim 4.4 \times 10^2$  monolayers of  $C_{60}$  molecules stacked by the (111) atomic planes of the fcc crystal [2,40]. Using the dimension of the film,  $\sim 12\text{ mm}$  in diameter, and the density of solid  $C_{60}$ ,  $1.6\text{ g cm}^{-3}$ , the amount of  $C_{60}$  contained in the sample film is estimated to be  $\sim 0.10\text{ mg}$ , equivalent to  $1.4 \times 10^{-7}\text{ mol}$  or  $8.2 \times 10^{16}$  molecules.

Figure 1 compares emission intensity of different  $T_{1u}$  modes of  $C_{60}$  at various temperatures in the range of  $27.4^\circ\text{C}-88.4^\circ\text{C}$ . The intensity of molecular IR emission bands increases by increasing temperature for  $T_{1u}(1)$  at  $526\text{ cm}^{-1}$ ,  $T_{1u}(2)$  at  $575\text{ cm}^{-1}$ ,  $T_{1u}(3)$  at  $1182\text{ cm}^{-1}$ , and  $T_{1u}(4)$  at  $1427\text{ cm}^{-1}$ . The intensity of the higher-frequency modes, namely,  $T_{1u}(3)$  and  $T_{1u}(4)$ , increases more signifi-

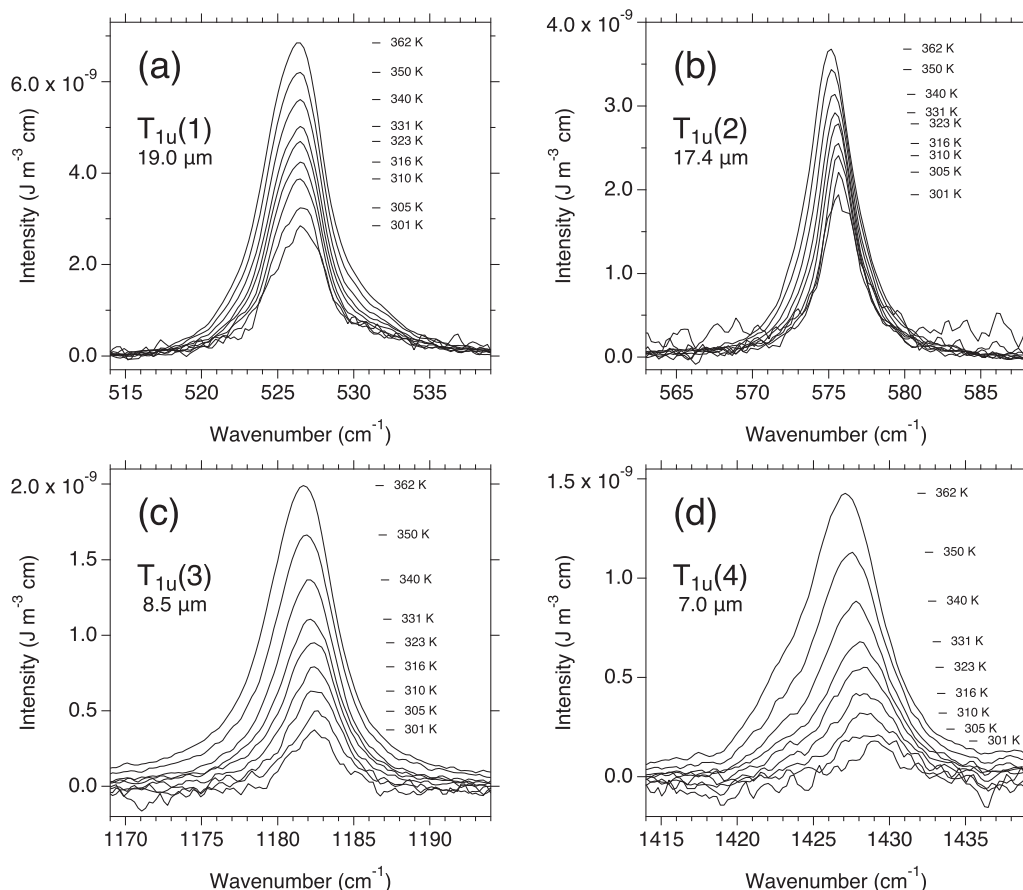


FIG. 2. IR emission bands for the  $T_{1u}$  modes of  $C_{60}$  at elevated temperatures.

cantly than the intensity of the lower-frequency modes,  $T_{1u}(1)$  and  $T_{1u}(2)$ .

Figure 2 depicts detailed band shapes of the IR emission for the four  $T_{1u}$  modes at different temperatures. A systematic increase in intensity is noted again for each band. Besides the lowest-frequency band of  $T_{1u}(1)$ , the intensity on the low-energy side of the band for the other three  $T_{1u}$  modes increases more strongly than the intensity on the high-energy side of the band with increasing temperature, and the peak downshifts accordingly by 1–2  $\text{cm}^{-1}$ . For actual molecules with anharmonicity, the distance between adjacent energy levels in the ladder of vibrationally excited states decreases for a pair of levels at higher excitation energy. The broadening of the band and the low-frequency shift of the peak by increasing temperature from 300 to 360 K indicate an increasing contribution of transitions between higher-energy combination and overtone levels where the transition energy slightly decreases via anharmonicity.

The band shape of  $T_{1u}(1)$  in Fig. 2(a) comprises a main band peaking at  $526.5 \text{ cm}^{-1}$  and a shoulder at  $525.0 \text{ cm}^{-1}$ . The latter feature is assignable to the band of the isotopologue, namely,  $^{13}\text{C}^{12}\text{C}_{59}$ , for which a  $^{12}\text{C}$  atom is substituted by a heavier isotope of  $^{13}\text{C}$  in a  $C_{60}$  cage [41,42]. For a random mixture of 60 carbon atoms with a natural isotopic abundance of 1.1%  $^{13}\text{C}$ , fractions of isotopologues are 51% for  $^{12}\text{C}_{60}$ , 34% for  $^{13}\text{C}^{12}\text{C}_{59}$ , 11% for  $^{13}\text{C}_2^{12}\text{C}_{58}$ , and 2.5% for  $^{13}\text{C}_3^{12}\text{C}_{57}$ . Thus, the second isotopologue,  $^{13}\text{C}^{12}\text{C}_{59}$  with  $C_s$

symmetry, amounts to two thirds of the major isotopologue,  $^{12}\text{C}_{60}$  with  $I_h$  symmetry. For  $C_s$ - $^{13}\text{C}^{12}\text{C}_{59}$ , the degeneracy of the  $v = 1$  level of  $T_{1u}(1)$  is lifted, and one of the three components of  $T_{1u}(1)$  downshifts in frequency by  $1.4 \text{ cm}^{-1}$ , as observed for the fundamental transition of  $^{13}\text{C}^{12}\text{C}_{59}$  isolated in solid parahydrogen,  $p\text{-H}_2$ , at cryogenic temperature [42]. It is comparable to the difference of  $\sim 1.5 \text{ cm}^{-1}$  between the peak and the shoulder for  $T_{1u}(1)$  in Fig. 2(a).

Fundamental transitions ( $v = 1 \leftarrow 0$ ) of  $T_{1u}$  modes of the major isotopologue of  $I_h$ - $^{12}\text{C}_{60}$  for matrix-isolated  $C_{60}$  in solid  $p\text{-H}_2$  are observed at  $529.77 \text{ cm}^{-1}$  for  $T_{1u}(1)$ , at  $578.24 \text{ cm}^{-1}$  for  $T_{1u}(2)$ , at  $1184.72 \text{ cm}^{-1}$  for  $T_{1u}(3)$ , and at  $1431.9 \text{ cm}^{-1}$  for  $T_{1u}(4)$  [42]. Downshifts of peaks for the emission bands of  $C_{60}$  at 300–360 K in Fig. 2 are  $\sim 3 \text{ cm}^{-1}$  for  $T_{1u}(1)$ , 2–3  $\text{cm}^{-1}$  for  $T_{1u}(2)$ , 2–3  $\text{cm}^{-1}$  for  $T_{1u}(3)$ , and 3–4.5  $\text{cm}^{-1}$  for  $T_{1u}(4)$ , depending on the emission temperatures, which are reasonably rationalized by anharmonicity peculiar to hot bands in transitions between highly excited vibrational states at elevated temperatures where the transition energy decreases.

Figure 3 plots integrated band intensity for the IR emission of  $T_{1u}(i)$  modes, with  $i = 1-4$ , for  $C_{60}$  at temperatures in the range of 301–362 K, which is obtained from the areal intensity of the emission band in Figs. 1 and 2. For ambient temperature at 301 K, the intensity of  $T_{1u}(3)$  relative to that of  $T_{1u}(1)$  is 0.15, whereas at the elevated temperature of 362 K, the ratio increases to 0.25. For  $T_{1u}(3)$ , the increase in intensity between 331 and 362 K is comparable to that between 301 and 331 K,

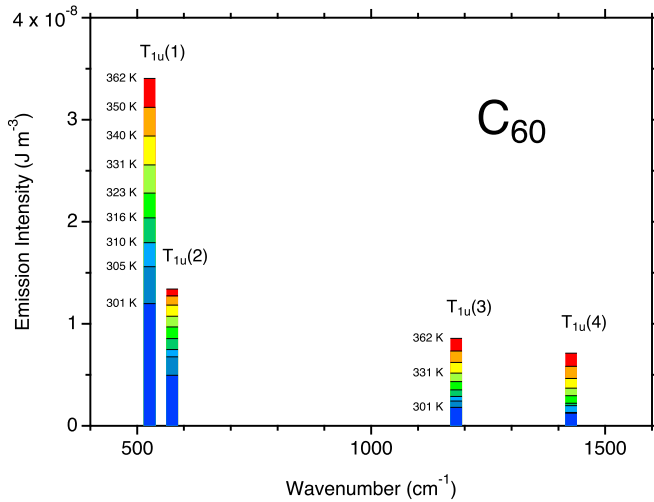


FIG. 3. Integrated intensity of the IR emission band for  $T_{1u}(i)$  modes, with  $i = 1-4$ , of the  $C_{60}$  thin film at temperatures in the range of 301–362 K.

whereas for  $T_{1u}(1)$ , the increase between 331 and 362 K is apparently smaller than that between 301 and 331 K, showing saturation. Table SIII compiles observed band intensity and relative intensity normalized to the intensity of  $T_{1u}(1)$  [30].

### B. Theoretical simulation

Figure 4 depicts the DOS for vibrationally excited states of  $I_h-C_{60}$  up to the excitation with  $v = 7$  vibrational energy quanta. In Fig. 4(a), the DOS of  $1.1 \times 10^{12}$  total states including degeneracy for  $1.5 \times 10^8$  distinct levels is plotted as a function of the excitation energy. Among them, 38.65% are states for which at least one energy quantum is assigned to the excitation of one of the four  $T_{1u}$  modes, namely, IR-emissive states. In Fig. 4(b), the IR-emissive states are classified further mode selectively into four  $T_{1u}$  modes and are plotted for each, i.e., 10.45% for  $T_{1u}(1)$ , 9.89% for  $T_{1u}(2)$ , 8.86% for  $T_{1u}(3)$ , and 9.46% for  $T_{1u}(4)$ . Reflecting the order of vibrational mode frequencies, the onset of the DOS for the lowest-frequency  $T_{1u}(1)$  mode lies lowest among the four  $T_{1u}$  modes. The onset of  $T_{1u}(2)$  follows almost the same pattern as  $T_{1u}(1)$ , whereas the onsets of  $T_{1u}(3)$  and  $T_{1u}(4)$  are shifted by  $\sim 1000 cm^{-1}$ , according to the difference in the vibrational mode frequencies. The difference in the percentage of the DOS for  $T_{1u}(i)$ , with  $i = 1-4$ , originates partly from the division of contributions for states in a combination level with the excitation of more than one  $T_{1u}$  mode because the band strength  $I_{IR}$  is different for the four  $T_{1u}$  modes as in Table I and the emission rate is competitive (see Appendix B).

The DOS function in general increases uniformly as a function of the excitation energy. The apparent maximum for each trace in Figs. 4(a) and 4(b) is artificial because of the limited number of vibrational energy quanta involved in the simulation. Since the lowest-frequency vibrational mode is fivefold  $H_g(1)$  with a harmonic frequency of  $266.17 cm^{-1}$  and since the excitation of up to seven vibrational quanta is considered in the simulation, the list of vibrational states is complete at only up to  $266.17 \times 7 = 1863 cm^{-1}$  and lacks states at higher excitation energies. As shown in the following

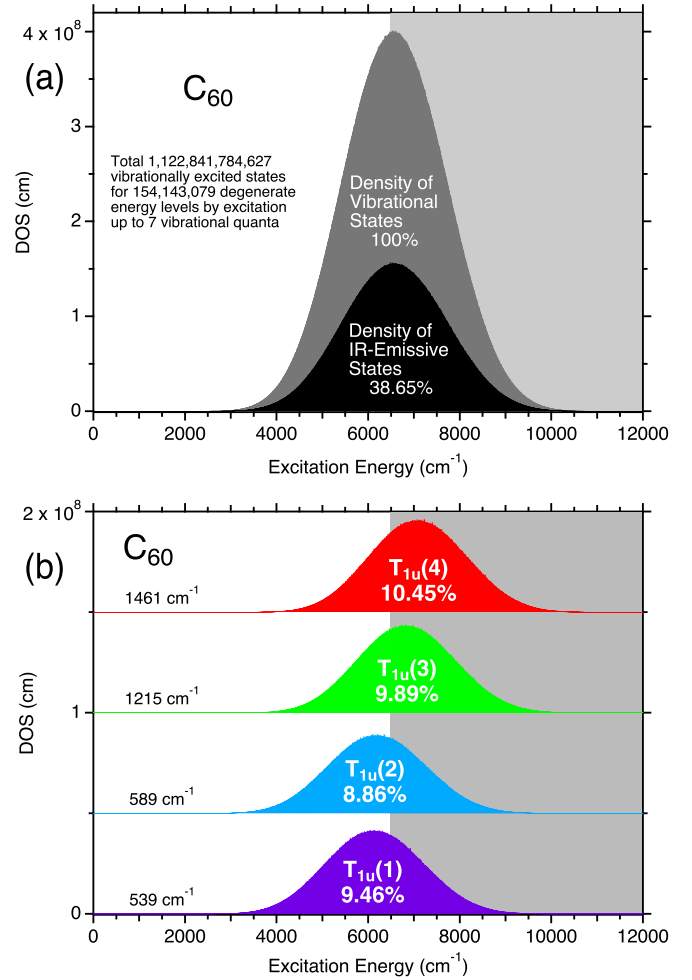


FIG. 4. Density of states (DOS) for vibrationally excited states in  $C_{60}$  up to the excitation with seven vibrational energy quanta. (a) DOS of a total of  $1.1 \times 10^{12}$  states including degeneracy for  $1.5 \times 10^8$  distinct levels of different excitation energies. (b) Mode-selective DOS for the four  $T_{1u}$  modes of  $C_{60}$ .

simulations, which should be compared with the experimental results for the temperature range of 300–360 K, populations in excited states with excitation energy up to  $\sim 6500 cm^{-1}$  are crucial, as indicated by shaded backgrounds in Figs. 4(a) and 4(b). With these situations in mind, interpretations of the results of the simulation should be carefully made.

In Figs. 5(a)–5(h), mode-selective IR emission intensity distributions for the four  $T_{1u}$  modes of  $C_{60}$  are compared at different temperatures in the range of 50–400 K, for which the Boltzmann distribution in vibrationally excited states is multiplied by the mode-dependent factor including the spontaneous emission rate  $A_{jk}$ , photon energy  $hc\tilde{\nu}$ , and Avogadro's number  $N_A$  and the factor is thus proportional to a cube of the vibrational frequency and the band strength,  $\propto \tilde{\nu}^3 I_{IR}$  [see Eqs. (6) and (7)]. The inset in each panel in Figs. 5(a)–5(h) shows the spectrum of integrated band intensity for the four  $T_{1u}$  modes at corresponding temperature.

First, at 50 K in Fig. 5(a), the excited-state population is limited at most in the vibrational  $v = 1$  level of the  $T_{1u}(1)$  and  $T_{1u}(2)$  modes, and the relative intensity of the emission

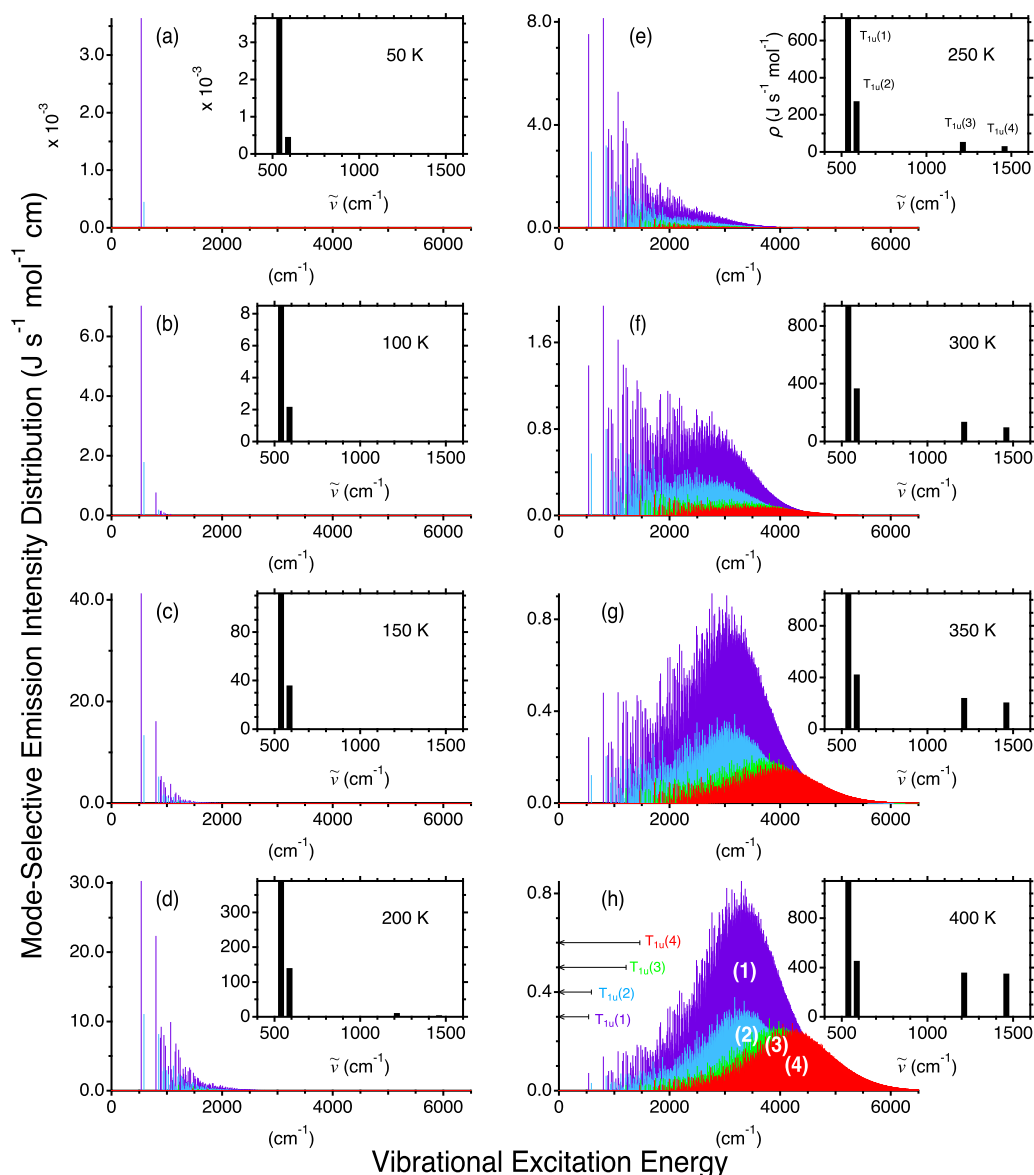


FIG. 5. Mode-selective IR emission intensity distribution at selected temperatures of 50–400 K for the four  $T_{1u}$  modes of  $C_{60}$  as a function of vibrational excitation energy. The inset in each panel shows the spectrum of integrated band intensity as a function of transition energy for the four  $T_{1u}$  modes at the corresponding temperature. In (h), arrows indicate fundamental transitions from  $v = 1$  to  $v = 0$  for the four  $T_{1u}$  modes.

for  $T_{1u}(2)$  is one eighth of that for  $T_{1u}(1)$ . The ground-state population predominates, and the IR emission is extremely weak at  $3.7 \times 10^{-3} \text{ J s}^{-1} \text{ mol}^{-1}$ . The signals of the emission of higher-frequency modes,  $T_{1u}(3)$  and  $T_{1u}(4)$ , are negligibly small. Second, by increasing temperature from 100 K [Fig. 5(b)] to 200 K [Fig. 5(d)], the absolute emission intensity for  $T_{1u}(1)$  increases from 8.5 to  $390 \text{ J s}^{-1} \text{ mol}^{-1}$ , and the relative intensity of  $T_{1u}(2)/T_{1u}(1)$  increases from 0.26 to 0.36 according to the increasing population in higher excitation energy levels up to  $2000 \text{ cm}^{-1}$ . Finally, as the population in higher excitation energy levels at  $2000\text{--}4000 \text{ cm}^{-1}$  increases above 250 K [Fig. 5(e)], the emission of the higher-frequency modes,  $T_{1u}(3)$  and  $T_{1u}(4)$ , appears, and the intensity increases more rapidly than for the lower-frequency modes,  $T_{1u}(1)$  and  $T_{1u}(2)$ . Under the condition of ambient temperature at 300 K [Fig. 5(f)], the weight of the population for vibrationally ex-

cited states shifts above  $2000 \text{ cm}^{-1}$ , and the contribution from populations in  $v = 1$  fundamental levels for 46 vibrational modes becomes negligible. Thus, above ambient temperature between 300 K [Fig. 5(f)] and 400 K [Fig. 5(h)], most transitions occur as hot bands between vibrationally excited states of various combinations and overtones. Note that simulated relative band intensity for  $T_{1u}(i)$ , with  $i = 1\text{--}4$ , at 350 K [Fig. 5(g)] is comparable to that observed for the IR emission of the  $C_{60}$  thin film at 350 K in Fig. 3.

The integrated emission band intensity for the simulated spectra in Fig. 5 is plotted as a function of temperature in Fig. 6(a) and superposed in the spectrum in Fig. 6(b). It is predicted that the molecular IR emission bands are missing below 100 K because most of the molecules are in the vibrational ground state. The IR emission of  $T_{1u}(1)$  and  $T_{1u}(2)$  predominates at temperatures between 100 and 200 K, and the

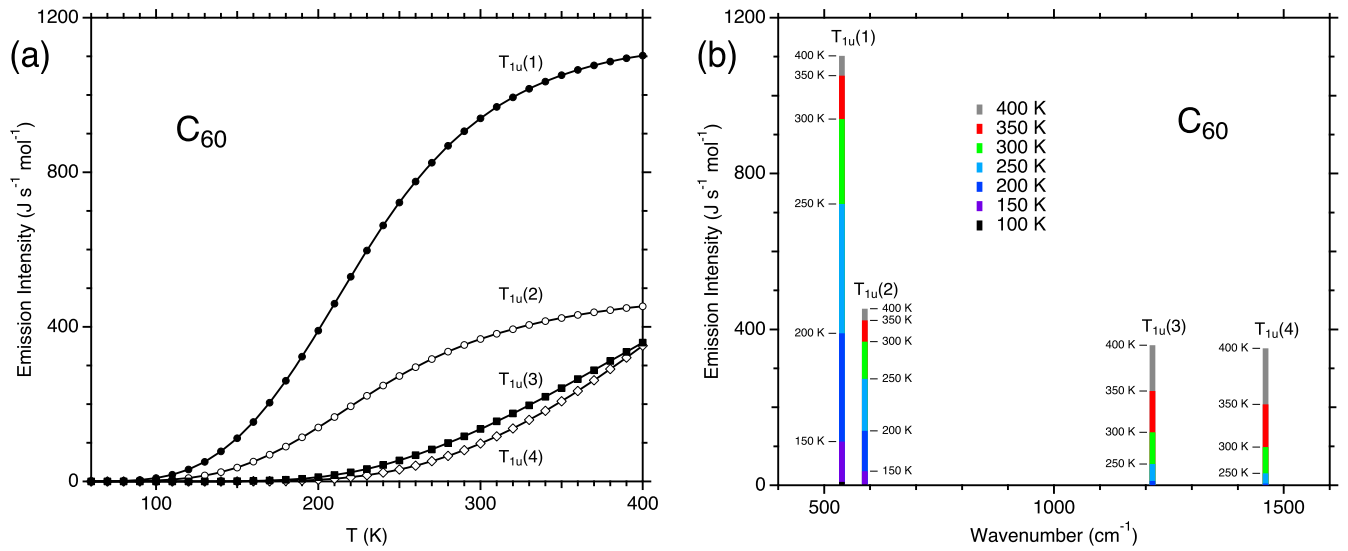


FIG. 6. Simulated IR emission band intensity for the four  $T_{1u}$  modes of  $C_{60}$  (a) as a function of temperature and (b) as merged in a single spectrum.

IR emission of  $T_{1u}(3)$  and  $T_{1u}(4)$  increases in intensity above 200 K. The intensity of  $T_{1u}(1)$  and  $T_{1u}(2)$  tends to saturate at 300–400 K, while the intensity of  $T_{1u}(3)$  and  $T_{1u}(4)$  constantly increases. The difference in the temperature dependence of the IR emission intensity leads to the difference in relative IR emission intensity, which can be exploited as a probe for the vibrational temperature of an ensemble of  $C_{60}$  molecules. Table SIII compiles theoretical band intensity and relative intensity normalized to the intensity of  $T_{1u}(1)$  [30].

### C. Comparison between experiment and theory

The experimental temperature dependence of the IR emission band intensity in Fig. 3 is compared with the theoretical simulation in Fig. 6(b). The spectral pattern of  $T_{1u}$  modes in Fig. 3 is well reproduced by the pattern in Fig. 6(b), although the expected effects of saturation for  $T_{1u}(1)$  and  $T_{1u}(2)$  and of rapid increase for  $T_{1u}(3)$  and  $T_{1u}(4)$  are not very clear in the observation in Fig. 3 compared to the theory in Fig. 6(b).

To avoid difficulty with calibration for absolute intensity, relative intensities between  $T_{1u}$  modes are compared as a function of temperature in Fig. 7. The high-frequency mode of  $T_{1u}(3)$  is a key feature for comparison with the low-frequency modes of  $T_{1u}(1)$  and  $T_{1u}(2)$ . Here, the observed IR emission band intensity for  $T_{1u}(i)$ , with  $i = 1-4$ , is normalized to that for  $T_{1u}(3)$  and plotted as a function of temperature in Fig. 7. The theoretical temperature dependence of the IR emission band intensity is also normalized to that for  $T_{1u}(3)$  and superposed in Fig. 7. With these plots and curves normalized to  $T_{1u}(3)$ , variations in the temperature dependence between different modes are pronounced.

In Fig. 7, the temperature-dependent experimental plots fit well with the theoretical curve. As the temperature increases in the range of 300–360 K, the intensity of  $T_{1u}(1)$  relative to  $T_{1u}(3)$  decreases from 7.0 to 4.0 for both the experiment and theory. Similarly, the experimental and theoretical intensities decrease from 2.8 to 1.6 for  $T_{1u}(2)$  and increase from 0.7 to 0.9 for  $T_{1u}(4)$ . These behaviors are rationalized qualitatively

because, for the emission of higher transition energy, populations in the excited states at higher energy levels are necessary, which requires higher temperature, as illustrated in Fig. 5.

## V. DISCUSSION

### A. Factors for further improvements

The present approach using the energy scale provides a consistent picture of the temperature dependence of the

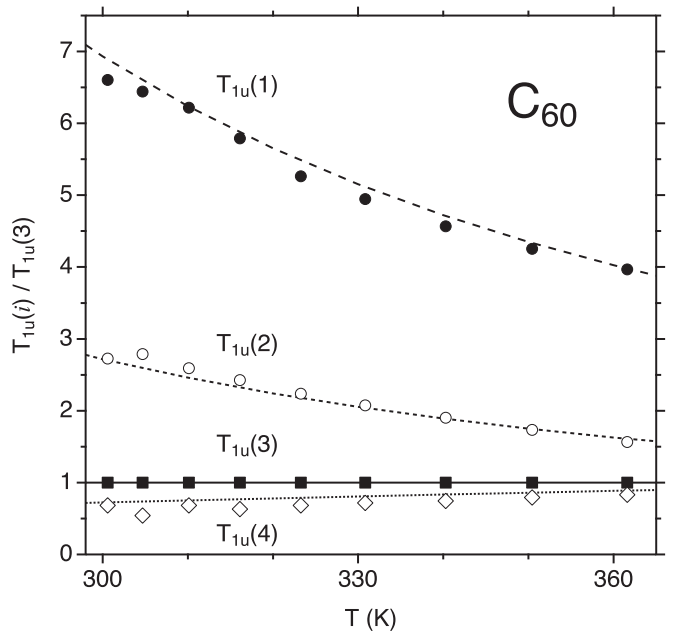


FIG. 7. Relative intensity for the IR emission bands of  $T_{1u}$  modes of  $C_{60}$  plotted as a function of temperature. The intensity is normalized for  $T_{1u}(3)$  to unity. The experimental plot (the theoretical curve) is solid circles (long-dashed line) for  $T_{1u}(1)$ , open circles (short-dashed line) for  $T_{1u}(2)$ , squares (solid line) for  $T_{1u}(3)$ , and diamonds (dotted line) for  $T_{1u}(4)$ .

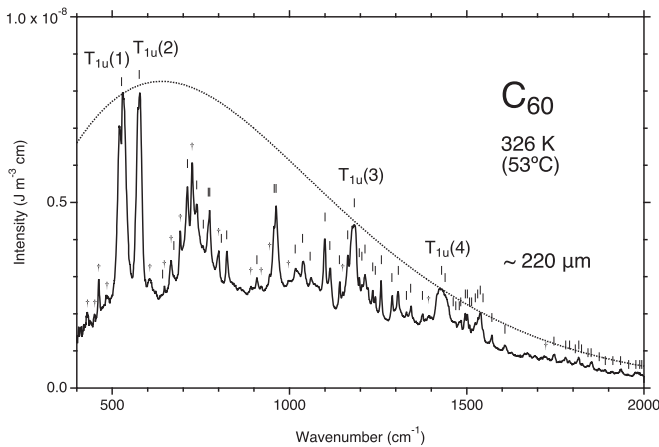


FIG. 8. IR emission spectrum of a 220  $\mu\text{m}$  disk of solid  $\text{C}_{60}$  at 326 K. The dotted line spectrum shows the blackbody radiation at the corresponding temperature.

IR emission band intensity of  $T_{1u}$  modes of  $\text{C}_{60}$ . The remaining issues are mentioned here for further improvement. The simulation is based on assumptions and approximations and also limited by computational feasibility. Does the limited number of excitation quanta under consideration, i.e., up to  $v = 7$ , cause any difference in the relative intensity of the IR emission of the  $T_{1u}$  modes? When the simulation is performed using excitations only up to  $v = 6$ , the absolute emission band intensity indeed deviates above 200 K, which lowers the curve of the simulation using excited states up to  $v = 7$  in Fig. 6(a). However, the curves for relative intensity are almost identical for both simulations using excitations up to  $v = 6$  and 7 in the whole range of temperatures, at least up to 400 K.

Harmonic frequencies are adopted for all the excited states, including fundamentals, overtones, and combinations, throughout the present simulation, as shown in Figs. 4–6. Does the anharmonicity correction improve the theoretical curve for the explanation of the experimental plots? The primary effect of the inclusion of anharmonicity is the downshift of vibrational frequencies at higher-energy excited levels in particular, typically by 2%–4% of the harmonic frequencies. Simple downshifts in frequency for all 46 vibrational normal modes realize the same Boltzmann distribution at lower temperature, leading to the shift toward low temperature of the theoretical curves for the mode-selective IR emission intensity in Fig. 6(a). Theoretical curves for the relative intensity in Fig. 7 also shift accordingly toward low temperature, although the agreement in the overall tendency between experiments and theory in Fig. 7 is fairly satisfactory without an anharmonicity correction.

### B. Effects of thickness of the sample

Finally, it is worthwhile to mention a sample with a different dimension. Figure 8 shows the IR emission spectrum of solid  $\text{C}_{60}$  at 326 K (solid line). The sample is a pressed disk of  $\text{C}_{60}$  powder with dimensions of 15 mm in diameter and about  $2.2 \times 10^2 \mu\text{m}$  in thickness. It is 400 times thicker than the thin film of  $\text{C}_{60}$  used for the experiments mentioned above. In Fig. 8, numerous emission peaks are discernible

even for the pristine  $\text{C}_{60}$ . Among them, bands of the four  $T_{1u}$  modes centered at 526, 575, 1182, and 1427  $\text{cm}^{-1}$  are extremely broadened and almost saturate at their peak intensities to the limit of blackbody radiation (dotted line). Even a dip is obvious for the band of  $T_{1u}(1)$ , implying self-absorption of the IR radiation at the frequency of strong absorption. The saturation of the emission intensity at the frequencies of the four IR-active  $T_{1u}$  modes occurs when the IR photon emitted toward the spectrometer by a  $\text{C}_{60}$  molecule near the backside of the sample disk is absorbed by another  $\text{C}_{60}$  molecule while traveling through the thickness of the sample disk of  $\text{C}_{60}$ . The only photons which come out of the sample disk to contribute to the emission spectrum are those emitted from  $\text{C}_{60}$  molecules located close to the front surface of the sample disk.

Most of the peaks other than the four  $T_{1u}$  modes in Fig. 8 are attributable to the emission bands of so-called higher-order infrared modes in combinations and overtones of the  $\text{C}_{60}$  molecule. Peaks with sticks are found to be identical by their frequencies and relative intensities with vibrational mode signals of weak absorption bands observed for a thin film of  $\text{C}_{60}$  with a thickness of 4  $\mu\text{m}$  [10]. These emission bands attributable to the higher-order IR modes are intrinsically weak compared to the electric dipole allowed transition of  $T_{1u}$  modes. Therefore, the condition for these bands is far from saturation; that is, the emitted photon from a  $\text{C}_{60}$  molecule near the backside even penetrates enough to come out of the sample disk and get detected by the spectrometer. As a consequence, the emission bands for the higher-order IR modes become conspicuous, as observed by the intensity comparable to the four saturating bands of the first-order IR-active  $T_{1u}$  modes. For relatively thick samples, quantitative evaluation of self-absorption is crucial for interpretation of the spectral intensity, where the optical thickness measured from the surface of the sample disk, i.e., the number of molecules under probe, differs from band to band for different vibrational mode frequencies and different intrinsic absorption intensities.

Peaks with daggers in Fig. 8 do not have counterparts in the absorption spectrum of the  $\text{C}_{60}$  thin film [10]. Most of them are distributed in a spectral range of relatively low frequencies below 1000  $\text{cm}^{-1}$ . These newly observed IR bands are possibly explained by transitions between highly excited vibrational states of combinations and overtones. For further understanding, detailed assignments will be discussed in future work.

## VI. CONCLUSIONS

The IR emission spectra of fullerene  $\text{C}_{60}$  thin films were measured, and theoretical simulations were performed for the spontaneous emission of the four vibrational  $T_{1u}$  modes by consideration of numerous vibrationally excited states, including fundamentals, overtones, and combinations at elevated temperatures. This work successfully provided a microscopic picture to understand how and why the IR emission spectrum of  $\text{C}_{60}$  changes with temperature within the framework of the thermal emission model. The results are applicable to the estimation of the vibrational temperature of  $\text{C}_{60}$  in stellar objects.

## ACKNOWLEDGMENTS

This work was supported by Grant-in-Aid for Scientific Research (C) No. JP20K05438 from the Japan Society for the Promotion of Science (JSPS). T.W. is grateful to Prof. T. Momose, The University of British Columbia (UBC), Canada, for his valuable comments on C<sub>60</sub> in solid parahydrogen. This paper is based upon work from COST Action CA21126 – Carbon nanostructures in space (NanoSpace), supported from European Cooperation in Science and Technology (COST).

## APPENDIX A: DEGENERACY OF OVERTONES

For a vibrational mode of  $n$ -fold degeneracy, e.g., for a threefold  $T_{1u}$  mode, the direct product of the same symmetry species results in a couple of symmetry species in  $n^2$  degrees of freedom. For the example of

$$T_{1u} \times T_{1u} = A_g + [T_{1g}] + H_g, \quad (\text{A1})$$

$3 \times 3 = 1 + 3 + 5 = 9$ . Among the resulting three symmetry species, the *antisymmetric product*, i.e.,  $T_{1g}$  in this case, is indicated in brackets as usual [34] to distinguish it from the other *symmetric products*, i.e.,  $A_g$  and  $H_g$ . For an *overtone* of a single degenerate mode, e.g.,  $T_{1u}(1) \times T_{1u}(1)$ , states of antisymmetric species do not exist, but states of symmetric species do exist, whereas for a *combination* of two distinctly different modes, even for a *combination* of the same symmetry species, e.g.,  $T_{1u}(1) \times T_{1u}(2)$ , states of both symmetric and antisymmetric species do exist.

APPENDIX B: DOS OF THE  $T_{1u}$  STATES

The state excited by two  $T_{1u}$  modes, namely, 1 and 2, decays as  $P_{12}(t) = P_{12}^{\text{(eq)}} e^{-(A_1+A_2)t}$ , where  $A_1$  and  $A_2$  denote spontaneous emission rates for the two modes. Although the depletion of the population is immediately compensated by thermal excitation under equilibrium to keep  $P_{12}(t) = P_{12}^{\text{(eq)}}$  constant, the instantaneous rate of depletion for the population of the state by IR emission, namely,  $R_{12}$ , is represented as

$$R_{12} = -\frac{dP_{12}}{dt} = A_1 P_{12} + A_2 P_{12} = R_{12}^{(1)} + R_{12}^{(2)}. \quad (\text{B1})$$

Contributions of the state decaying to lower states by the IR emission through the  $T_{1u}$  modes, 1 and 2, are counted, respectively, as

$$\frac{R_{12}^{(1)}}{R_{12}} = \frac{A_1}{A_1 + A_2}, \quad \frac{R_{12}^{(2)}}{R_{12}} = \frac{A_2}{A_1 + A_2}. \quad (\text{B2})$$

With this convention, a total contribution of the state is unity irrespective of the number of  $T_{1u}$  modes for the excitation of the state. Thus, a double count of the state is avoided, and the total number of excited states is conserved consistently for both the mode-selective DOS of the IR-emissive states and the DOS of all the vibrational states.

- 
- [1] H. W. Kroto, J. R. Heath, S. C. O'Brien, R. F. Curl, and R. E. Smalley, C<sub>60</sub>: Buckminsterfullerene, *Nature (London)* **318**, 162 (1985).
- [2] W. Krätschmer, L. D. Lamb, K. Fostiropoulos, and D. R. Huffman, Solid C<sub>60</sub>: A new form of carbon, *Nature (London)* **347**, 354 (1990).
- [3] W. Krätschmer, K. Fostiropoulos, and D. R. Huffman, The infrared and ultraviolet absorption spectra of laboratory-produced carbon dust: Evidence for the presence of the C<sub>60</sub> molecule, *Chem. Phys. Lett.* **170**, 167 (1990).
- [4] J. Cami, J. Bernard-Salas, E. Peeters, and S. E. Malek, Detection of C<sub>60</sub> and C<sub>70</sub> in a young planetary nebula, *Science* **329**, 1180 (2010).
- [5] E. K. Campbell, M. Holtz, D. Gerlich, and J. P. Maier, Laboratory confirmation of C<sub>60</sub><sup>+</sup> as the carrier of two diffuse interstellar bands, *Nature (London)* **523**, 322 (2015).
- [6] B. H. Foing and P. Ehrenfreund, Detection of two interstellar absorption bands coincident with spectral features of C<sub>60</sub><sup>+</sup>, *Nature (London)* **369**, 296 (1994).
- [7] E. Osawa, Superaromaticity [in Japanese], *Kagaku* **25**, 854 (1970).
- [8] B. Chase, N. Herron, and E. Holler, Vibrational spectroscopy of fullerenes (C<sub>60</sub> and C<sub>70</sub>). Temperature dependent studies, *J. Phys. Chem.* **96**, 4262 (1992).
- [9] D. Dixon, B. E. Chase, G. Fitzgerald, and N. Matsuzawa, Prediction of the fundamental vibrational frequencies for C<sub>60</sub> by local density functional theory, *J. Phys. Chem.* **99**, 4486 (1995).
- [10] K.-A. Wang, A. M. Rao, P. C. Eklund, M. S. Dresselhaus, and G. Dresselhaus, Observation of higher-order infrared modes in solid C<sub>60</sub> films, *Phys. Rev. B* **48**, 11375 (1993).
- [11] A. M. Vassallo, L. S. K. Pang, P. A. Cole-Klarke, and M. A. Wilson, Emission FTIR study of C<sub>60</sub> thermal stability and oxidation, *J. Am. Chem. Soc.* **113**, 7820 (1991).
- [12] C. I. Frum, R. Engleman, Jr., H. G. Hedderich, P. F. Bernath, L. D. Lamb, and D. R. Huffman, The infrared emission spectrum of gas-phase C<sub>60</sub> (buckminsterfullerene), *Chem. Phys. Lett.* **176**, 504 (1991).
- [13] L. Nemes, R. S. Ram, P. F. Bernath, F. A. Tinker, M. C. Zumwalt, L. D. Lamb, and D. R. Huffman, Gas-phase infrared emission spectra of C<sub>60</sub> and C<sub>70</sub>. Temperature-dependent studies, *Chem. Phys. Lett.* **218**, 295 (1994).
- [14] D. A. García-Hernández, A. Machado, P. García-Lario, L. Stanghellini, E. Villaver, R. A. Shaw, R. Szczerba, and J. V. Perea-Carderón, Formation of fullerenes in H-containing planetary nebulae, *Astrophys. J.* **724**, L39 (2010).
- [15] K. Sellgren, M. W. Werner, J. G. Ingalls, J. D. T. Smith, T. M. Carleton, and C. Joblin, C<sub>60</sub> in reflection nebulae, *Astrophys. J.* **722**, L54 (2010).
- [16] Y. Zhang and S. Kwok, Detection of C<sub>60</sub> in the protoplanetary nebula IRAS 01005+7910, *Astrophys. J.* **730**, 126 (2011).
- [17] D. A. García-Hernández, N. K. Rao, and D. L. Lambert, Are C<sub>60</sub> molecules detectable in circumstellar shells of R Coronae Borealis stars? *Astrophys. J.* **729**, 126 (2011).
- [18] D. A. García-Hernández, S. Iglesias-Groth, J. A. Acosta-Pulido, A. Machado, P. García-Lario, L. Stanghellini, E. Villaver,

- R. A. Shaw, and F. Cataldo, The formation of fullerenes: Clues from new  $C_{60}$ ,  $C_{70}$ , and (possible) planar  $C_{24}$  detections in Magellanic Cloud planetary nebulae, *Astrophys. J.* **737**, L30 (2011).
- [19] G. C. Clayton, O. D. Marco, B. A. Whitney, B. Babler, J. S. Gallagher, J. Nordhaus, A. K. Speck, M. J. Wolff, W. R. Freeman, K. A. Camp, W. A. Lawson, J. Roman-Duval, K. A. Misselt, M. Meade, G. Sonneborn, M. Matsuura, and M. Meixner, The dust properties of two hot R Coronae Borealis stars and a Wolf-Rayet central star of a planetary nebulae: In search of a possible link, *Astron. J.* **142**, 54 (2011).
- [20] C. Gielen, J. Cami, J. Bouwman, E. Peeters, and M. Min, Carbonaceous molecules in the oxygen-rich circumstellar environment of binary post-AGB stars:  $C_{60}$  fullerenes and polycyclic aromatic hydrocarbons, *Astron. Astrophys.* **536**, A54 (2011).
- [21] K. R. G. Roberts, K. T. Smith, and P. J. Sarre, Detection of  $C_{60}$  in embedded young stellar objects, a Herbig Ae/Be star and an unusual post-asymptotic giant branch star, *Mon. Not. R. Astron. Soc.* **421**, 3277 (2012).
- [22] O. Berne and A. G. G. M. Tielens, Formation of buckminsterfullerene ( $C_{60}$ ) in interstellar space, *Proc. Natl. Acad. Sci. USA* **109**, 401 (2012).
- [23] E. R. Micelotta, A. P. Jones, J. Cami, E. Peeters, J. Bernard-Salas, and G. Fanchini, The formation of cosmic fullerenes from arophanic clusters, *Astrophys. J.* **761**, 35 (2012).
- [24] Y. Zhang and S. Kwok, On the detections of  $C_{60}$  and derivatives in circumstellar environments, *Earth Planets Space* **65**, 1069 (2013).
- [25] J. Bernard-Salas, J. Cami, E. Peeters, A. P. Jones, E. R. Micelotta, and M. A. T. Groenewegen, On the excitation and formation of circumstellar fullerenes, *Astrophys. J.* **757**, 41 (2012).
- [26] M. Otsuka, F. Kemper, J. Cami, E. Peeters, and J. Bernard-Salas, Physical properties of fullerene-containing galactic planetary nebulae, *Mon. Not. R. Astron. Soc.* **437**, 2577 (2014).
- [27] A. C. Brieva, R. Gredel, C. Jäger, F. Huisken, and T. Henning,  $C_{60}$  as a probe for astrophysical environments, *Astrophys. J.* **826**, 122 (2016).
- [28] S. Iglesias-Groth, F. Cataldo, and A. Manchado, Infrared spectroscopy and integrated molar absorptivity of  $C_{60}$  and  $C_{70}$  fullerenes at extreme temperatures, *Mon. Not. R. Astron. Soc.* **413**, 213 (2011).
- [29] S. Iglesias-Groth, D. A. García-Hernández, F. Cataldo, and A. Manchado, Infrared spectroscopy of hydrogenated fullerenes (fulleranes) at extreme temperatures, *Mon. Not. R. Astron. Soc.* **423**, 2868 (2012).
- [30] See Supplemental Material at <http://link.aps.org/supplemental/10.1103/PhysRevB.109.035409> for the experimental details, i.e., the setup of the measurement of IR emission spectra in Fig. S1 and the typical IR absorption and emission spectra of the  $C_{60}$  thin film in Fig. S2. Reference [11] is also cited in relation to the difference in processing the spectral intensity. Numerical data for the theoretical simulation are also found in Tables SI and SII. The IR emission band intensities obtained for the experimental and theoretical results are compiled in Table SIII.
- [31] G. Herzberg, *Molecular Spectra and Molecular Structure*, 2nd ed. (Krieger, Malabar, FL, 1950), Vol. 1, p. 20.
- [32] R. C. Hilborn, Einstein coefficients, cross sections, f values, dipole moments, and all that, *Am. J. Phys.* **50**, 982 (1982).
- [33] E. R. Cohen, T. Cvitaš, J. G. Frey, B. Holmström, K. Kuchitsu, R. Marquardt, I. Mills, F. Pavese, M. Quack, J. Stohner, H. Strauss, M. Takami, and A. J. Thor, *Quantities, Units, and Symbols in Physical Chemistry, IUPAC Green Book*, 3rd ed. (RSC Publishing, Cambridge, 2007).
- [34] P. F. Bernath, *Spectra of Atoms and Molecules*, 3rd ed. (Oxford University Press, Oxford, 2016), p. 290.
- [35] K. Yamasaki, *Einstein Coefficients A and B* [in Japanese], 5th ed., Physical Chemistry Monograph Series Vol. 26 (Hiroshima University Institutional Repository, Higashi-Hiroshima, Japan, 2019).
- [36] J. Spanget-Larsen, IR intensity: Lorentz epsilon curve from 'Gaussian' FREQ output (2015), doi: [10.13140/RG.2.1.4181.6160](https://doi.org/10.13140/RG.2.1.4181.6160).
- [37] M. J. Frisch *et al.*, *GAUSSIAN 16, revision C.01*, Gaussian, Inc., Wallingford, CT, 2019.
- [38] J. E. Bright Wilson, D. C. Decius, and P. C. Cross, *Molecular Vibrations* (Dover, New York, 1955), p. 153.
- [39] K. Yamasaki, *Irreducible Representation of Vibrational Levels* [in Japanese], 3rd ed., Physical Chemistry Monograph Series Vol. 28 (Hiroshima University Institutional Repository, Higashi-Hiroshima, Japan, 2019).
- [40] P. A. Heiney, J. E. Fischer, A. R. McGhie, W. J. Romanow, A. M. Denenstein, J. P. McCauley, Jr., A. B. Smith, and D. E. Cox, Orientational ordering transition in solid  $C_{60}$ , *Phys. Rev. Lett.* **66**, 2911 (1991).
- [41] N. Sogoshi, Y. Kato, T. Wakabayashi, T. Momose, S. Tam, M. E. DeRose, and M. E. Fajardo, High-resolution infrared absorption spectroscopy of  $C_{60}$  molecules and clusters in parahydrogen solids, *J. Phys. Chem. A* **104**, 3733 (2000).
- [42] T. Wakabayashi, T. Momose, and M. E. Fajardo, Matrix isolation spectroscopy and spectral simulations of isotopically substituted  $C_{60}$  molecules, *J. Chem. Phys.* **151**, 234301 (2019).